Supporting Information

Tris-amido Naphthoquinone: Toward High Capacity and Stability Organic Cathode for Aqueous Zinc Battery

Jia Cai[1], Sen Zhang[1], Jing Qin[1], Qianglong Chen[1], Hao Jing[3], Xiujuan Wang[1,2], Xiaoming He[1]**

[1] Key Laboratory of Applied Surface and Colloid Chemistry (Ministry of Education), School of Chemistry and Chemical Engineering, Shaanxi Normal University, Xi'an 710119, P.R. China

[2] Key Laboratory of Hexi Corridor Resources Utilization of Gansu, Hexi University, Zhangye 734000, PR China

[3] State Key Laboratory of Photon-Technology in Western China Energy International Collaborative Center on Photoelectric Technology and Nano Functional Materials Institute of Photonics & Photon-Technology, Northwest University, Xi'an 710127, PR China

*Corresponding Author Email: xjwang@snnu.edu.cn, xmhe@snnu.edu.cn

1. Materials and Instruments

Benzoyl chloride, terephthaloyl chloride, 1,3,5-Benzenetricarboxylic acid chloride, methoxyammonium chloride, potassium carbonate (K_2CO_3), zinc trifluoromethanesulfonate ($Zn(CF_3SO_3)_2$, >98%) 1,4-naphthoquinone, ethyldiisopropylamine ($^iPr_2NEt$), acetonitrile, N,N-Dimethylformamide (DMF), dichloromethane (DCM), poly(vinyl alcohol) (PVA (85-90 mol% hydrolyzed); Mw: 8200), urea, zinc sulfate heptahydrate ($ZnSO_4 \cdot 7H_2O$, ⩾99%) were purchased from Adamas, Alfa Aesar, Aldrich and Energychemical. polytetrafluoroethylene (PTFE) emulsion was purchased from Tianjin Anuohe New Energy Technology Co. Ltd. Carbon black (ECP-600JD) was purchased from Shenzhen Kejing Zhida Technology Co. Ltd. Zinc metal foil was purchased from Qinghe Jiarun Metal Materials Co. Ltd. CR2032 battery case and separator were obtained from DoDoChem. Unless otherwise stated, all other reagents or solvents were used without purification.

^1H NMR and ^{13}C NMR spectra were recorded on 600 MHz BRUKER spectrometers. IR spectra were obtained on a PE-Frontier instrument. Ultraviolet-visible (UV-vis) absorption spectra were obtained on Cary 3500 spectrometer. Scanning electron microscope (SEM) images were recorded using a Hitachi SU8220 system. Powder X-ray diffraction (PXRD) patterns were recorded on a Bruker D8 Advance instrument. Thermogravimetric analysis (TGA) was performed under a nitrogen atmosphere from 25 to 800 ℃ with a heating rate of 10 ℃ min^{-1}. The X-ray photoelectron spectra (XPS) experiments were carried out on a PHI-5400 electron spectrometer. Theoretical calculations were carried out at the B3LYP/6-31G (d, p) level by using the GAUSSIAN 09 suite of programs.[S1]

3. Synthesis

Synthesis of MANQ.

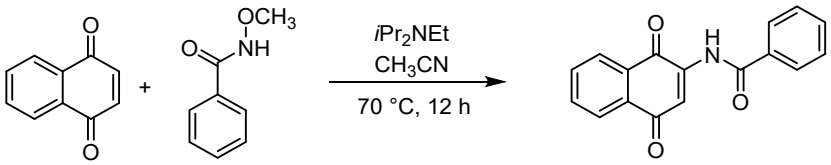

A mixture of 1,4-naphthoquinone (2.1 g, 12 mmol), *N*-methoxybenzamide (1.8 g, 12 mmol), *i*Pr_2NEt (3.1 g, 24 mmol) in CH_3CN (80 mL) was stirred in at 70 ºC for 12 hours. After removal of volatiles under vacuum, the residues were purified on silica flash column with AcOEt/hexane (1:10, v/v) as eluents to obtain the final product as brown solid (Yield: 91 %). ^{1}H NMR (600 MHz, $CDCl_3$): δ (ppm) = 9.21 (s, 1H), 8.15 (t, J = 7.8 Hz, 2H), 8.03 (s, 1H), 7.95 (d, J = 7.8 Hz, 2H), 7.81 (t, J = 7.8 Hz, 1H), 7.75 (t, J = 7.8 Hz, 1H), 7.62 (t, J = 7.8 Hz, 1H), 7.55 (t, J = 7.8 Hz, 2H). ^{13}C NMR (150 MHz, $CDCl_3$): δ (ppm) = 185.15, 181.23, 165.82, 140.13, 135.07, 133.32, 133.27, 132.97, 132.30, 130.00, 129.07, 127.36, 126.72, 126.48, 117.31. HR-MS: m/z calculated for $C_{17}H_{12}NO_3^+$ $[M+H]^+$ 278.0812, found 278.0814.

Synthesis of TANQ.

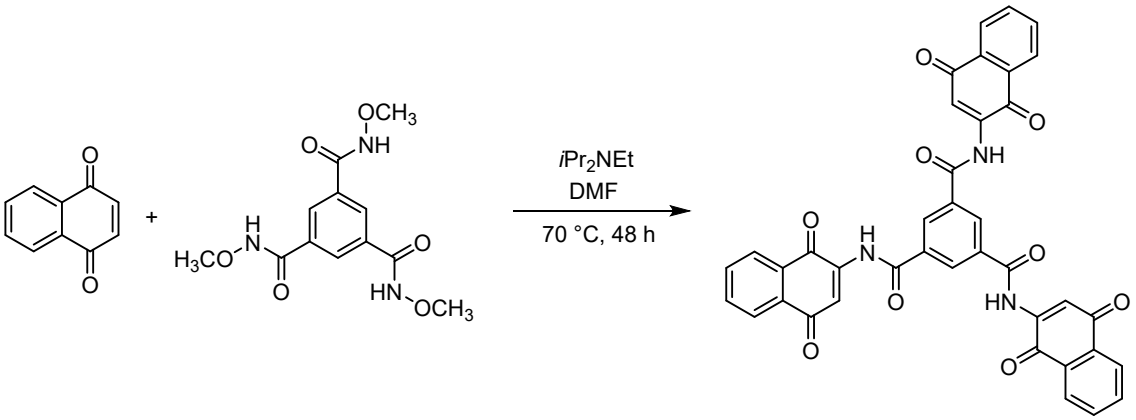

A mixture of 1,4-naphthoquinone (15.8 g, 100 mol), N', N'', N'''-trimethoxy-1,3,5-tricarboxamide (4.95 g, 16.7 mmol), *i*Pr_2NEt (26 mL, 150 mmol) in DMF (250 mL) was stirred in at 70 ºC for 48 hours under N_2. The resulting precipitate was collected by hot filtration, washed with DMF, EtOH and THF. The products were dried *in vacuo* for 24 h. Yield: 57 %. ^{1}H NMR (600 MHz, $CDCl_3$/CF_3COOD (9:1, v/v)): δ (ppm) = 9.60 (s, 3H), 8.81 (s, 3H), 8.22-8.18 (m, 6H), 8.12 (s, 3H), 7.92-7.85 (m, 6H). ^{13}C NMR (150 MHz, $CDCl_3$/CF_3COOD (9:1, v/v)): δ (ppm) = 188.96, 180.38, 166.40, 140.84, 135.96, 135.08, 134.59, 131.47, 131.39, 129.70, 127.61, 127.26, 118.38.

3. Battery Fabrication and Testing

The working electrodes were prepared by mixing the TANQ or MANQ, conductive carbon black (ECP-600JD) and polytetrafluoroethylene (PTFE) with a mass ratio of 6/3/1 (unless other noted) using H_2O as dispersion solvent. Noted that 60 wt.% polytetrafluoroethylene (PTFE) dispersion in H_2O was used. Then the slurry was compressed into discs and pressed onto stainless-steel mesh. The mass loading of the active materials was *ca.* 1.0 mg cm^{-2}. The fully prepared electrodes were then dried at 80 °C for 12 h in a vacuum oven to remove any residual solvent.

To construct zinc-organic batteries, TANQ or MANQ based cathode, 2 M aqueous $Zn(CF_3SO_3)_2$ electrolyte, Zn metal anode (> 99.99% purity), and glass fiber separator were packaged into CR2032 coin-type cells. The battery was left to stand for 12 hours before testing. The battery performance data were measured on a LAND CT2001A battery system at 30 °C with the voltage range of 0.1-1.6V. Cyclic voltammetry (CV) and electrochemical impedance spectroscopy (EIS) tests of the batteries were performed on a CHI760E electrochemical workstation. To perform the galvanostatic intermittent titration technique (GITT), the cells were subjected to 10-minute charge/discharge pulses at a constant

current, with 30-minute intervals for voltage relaxation, using cut-off voltages of 1.6 V (charge) and 0.1 V (discharge).

4. Calculations of the Electrochemical Metrics

Theoretical capacity (C_{theor}, mAh g^{-1}) was calculated according to the equation (1):

$$C_{theor} = \frac{nF}{3.6 \times M} \quad (1)$$

where n is the number of electrons transferred per molecules, F is the Faraday's constant (96484 C mol^{-1}), M is molecular weight of the molecules.

The b-value and capacitive contribution at a particular potential were determined as follows:

The relationship between scan rate (υ, mV s^{-1}) in a CV and the corresponding cathodic or anodic peak current (i_p, A g^{-1}) is shown in equation (2).[S2] The b-value was the slope of the log(v)-log(i_p) plots according to equation (3).

$$i_p = av^b \quad (2)$$

$$\log(i_p) = \log(a) + b\log(v) \quad (3)$$

where a and b are adjustable parameters.

Moreover, the relationship between the current at a particular potential (i(V), A g^{-1}) and the scan rate (υ, mV s^{-1}) is shown in equation (4).[S3] Solving for the values of k_1 and k_2 at each potential, we can obtain the percentage of capacitive contribution the total current (k_2v/i(V)).

$$i(V) = k_1v^{1/2} + k_2v \quad (4)$$

5. Calculation of apparent ion diffusion coefficients (D_{app}, $cm^2\ s^{-1}$) from GITT

The apparent diffusion coefficients (D_{app}) are calculated by the following equation: [S4]

$$D_{app} = \frac{4}{\pi\tau}\left(\frac{V_m m_B}{SM_m}\right)^2\left(\frac{\Delta E_s}{\Delta E_t}\right)^2 \quad (6)$$

where D_{app} is the apparent ion diffusion coefficient ($cm^2\ s^{-1}$), τ is the the duration of the current pulse (s), V_m is the molar volume of the active material ($cm^3\ mol^{-1}$), m_B is the mass of the active material in the electrolyte (g), M_m is the molar mass of active material ($g\ mol^{-1}$), S is the contact surface area (cm^2) between electrode and electrolyte, ΔE_s is the equilibrium potential change induced by current pulse, ΔE_t is the potential variation during the constant current pulse.

6. Supplementary Tables and Figures.

Table S1. Summary of half-cell ZOB performances based on MANQ and TANQ.

Materials	Theor. e numbers	C_{theor} (mAh g^{-1})	Rate performance: Capacity (mAh g^{-1}) Current density	Cycle Stability: Capacity (mAh g^{-1}) / retention / cycles / current density (A g^{-1})
MANQ	2	193	161, 125, 99, 86, 78, 74 0.1, 0.2, 0.5, 1.0, 2.0, 3.0	97/59%/250/0.2 72/72%/700/2
TANQ	6	238	213, 203, 190, 176, 153, 132 0.1, 0.2, 0.5, 1.0, 2.0, 3.0	174/80%/250/0.2 130/94%/700/2

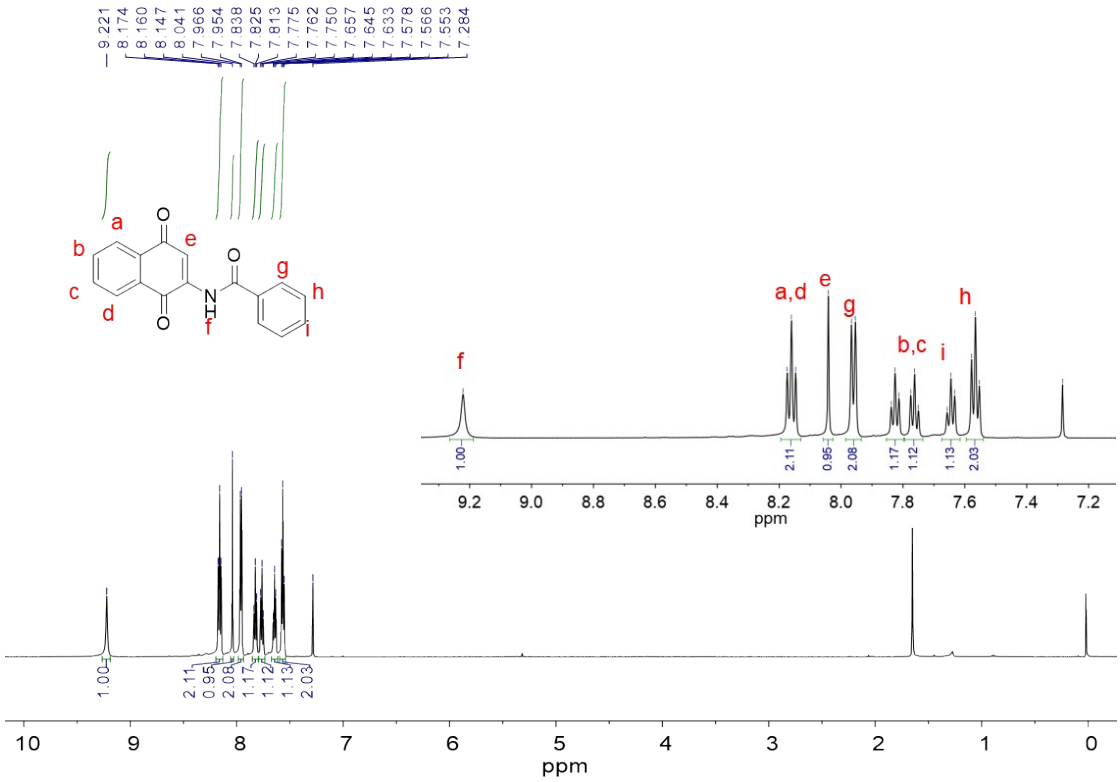

Figure S1. ^{1}H NMR spectra of MANQ in $CDCl_3$ at 298 K.

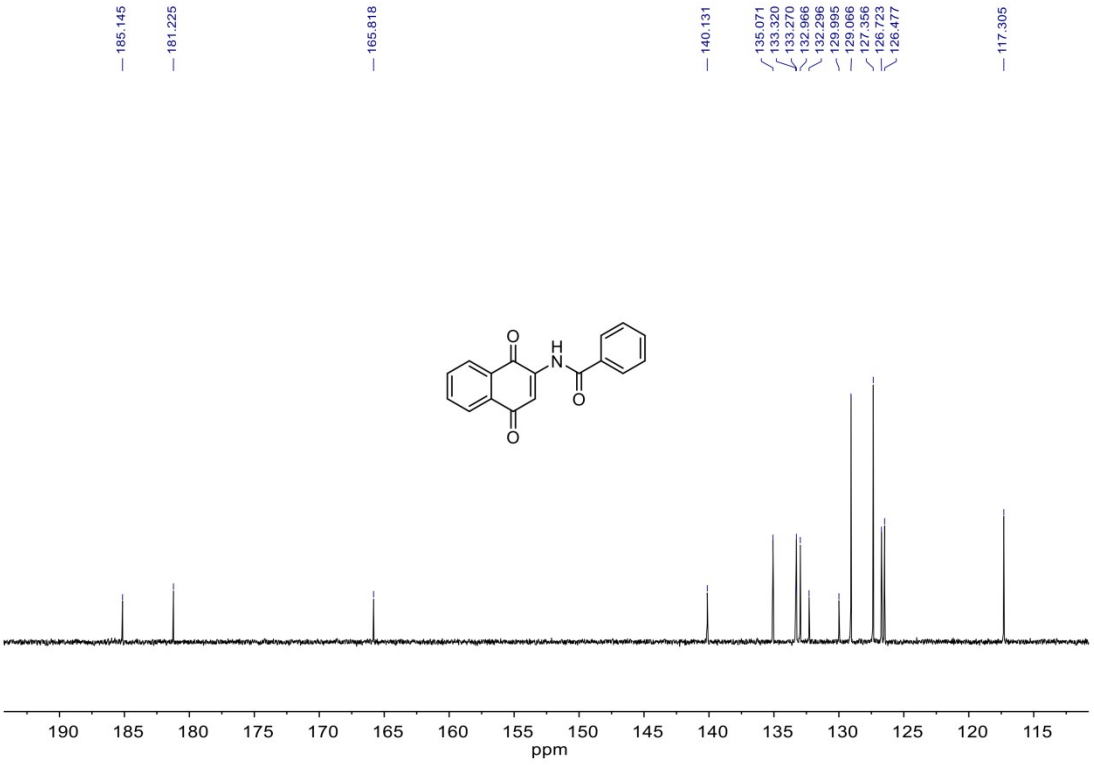

Figure S2. ^{13}C NMR spectrum of MANQ in $CDCl_3$.

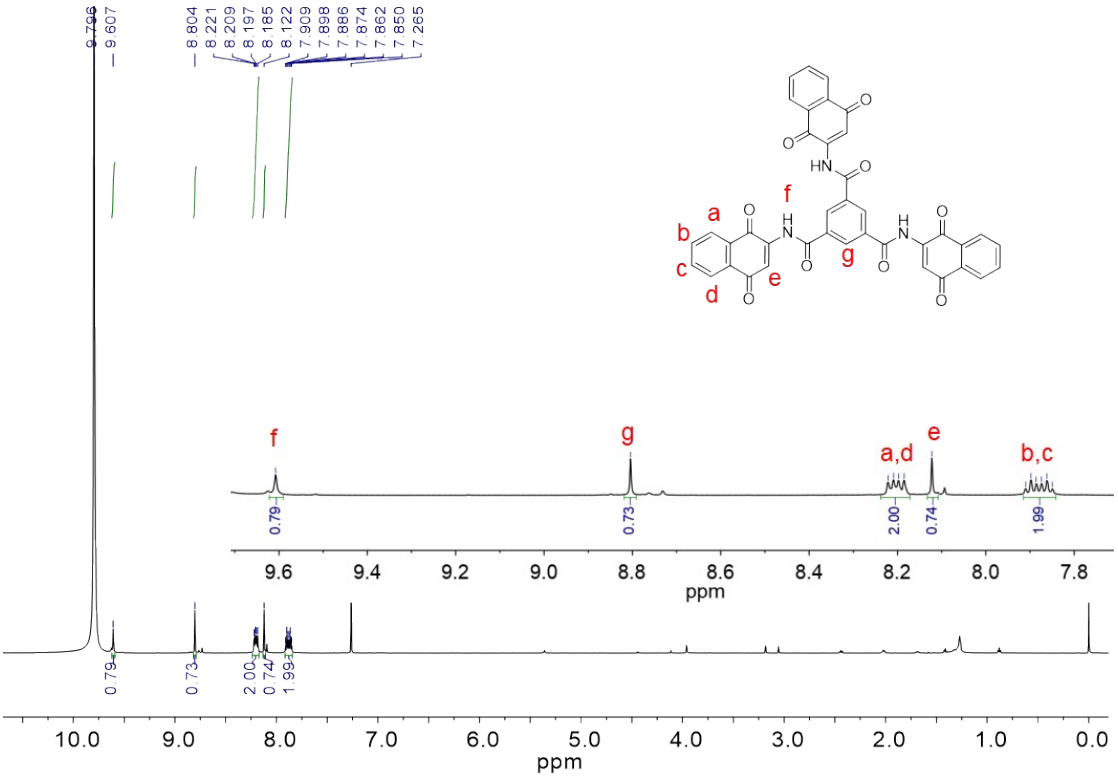

Figure S3. ^{1}H NMR spectrum of TANQ in $CDCl_3$ with 5% CF_3COOD at 298 K.

Note: TANQ is not soluble in $CDCl_3$. Addition of CF_3COOD can break the hydrogen bond to promote the solubility.

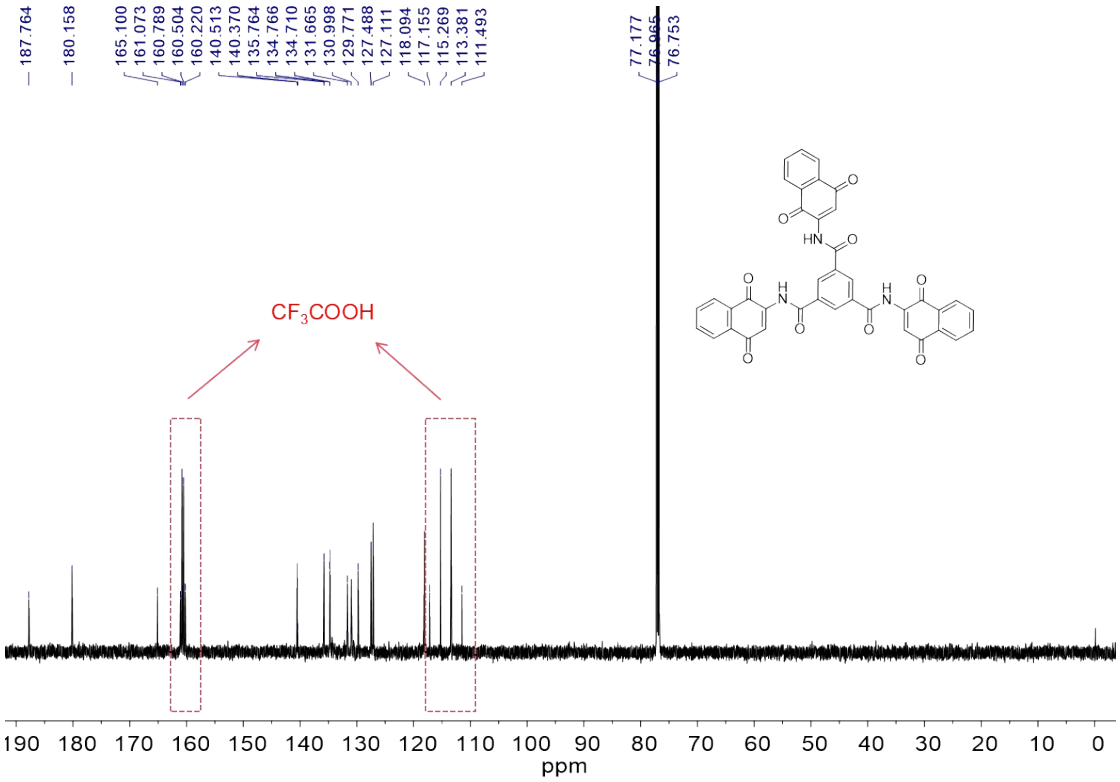

Figure S4. ^{13}C NMR spectrum of TANQ in $CDCl_3$ with 5% CF_3COOD at 298 K.

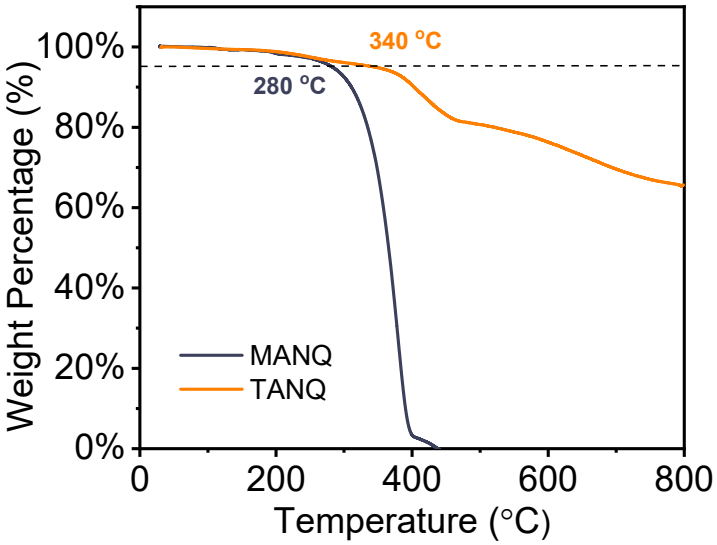

Figure S5. Thermal gravimetric analysis (TGA) profiles of TANQ and MANQ.

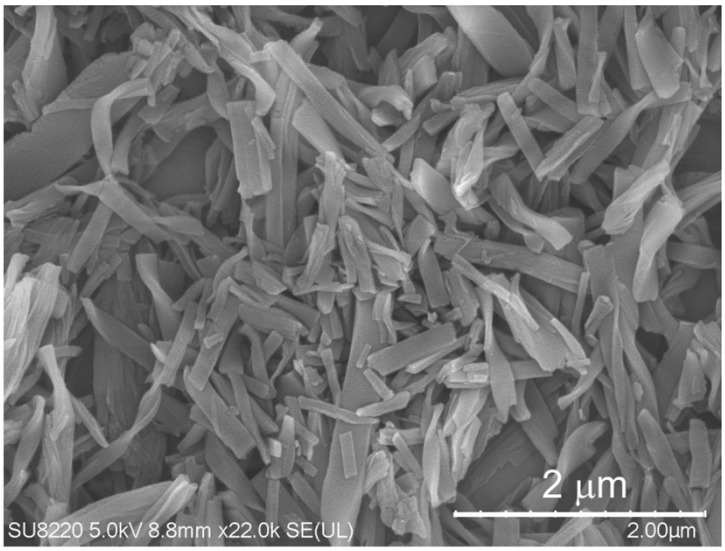

Figure S6. SEM image of TANQ.

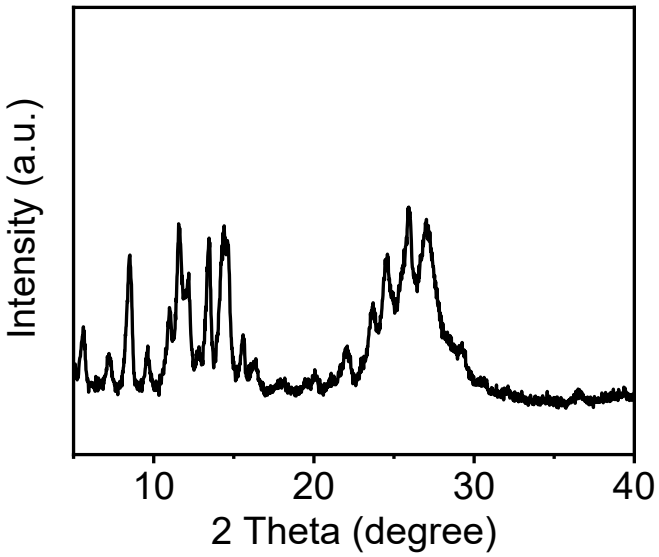

Figure S7. XRD patterns of TANQ.

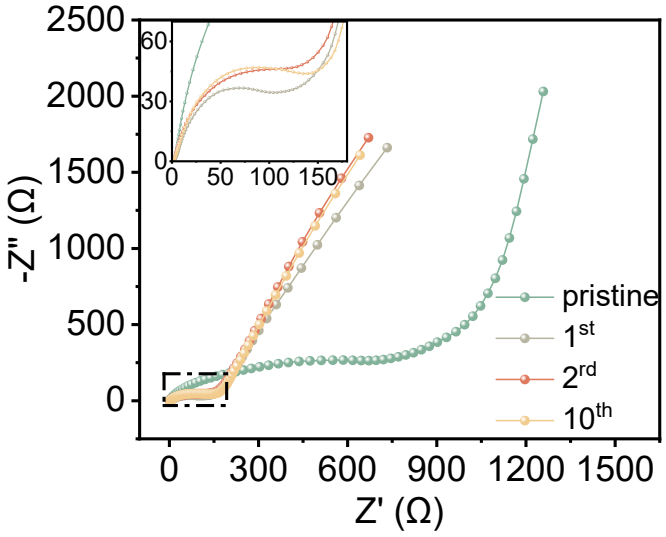

Figure S8. EIS curves of TANQ at different cycles.

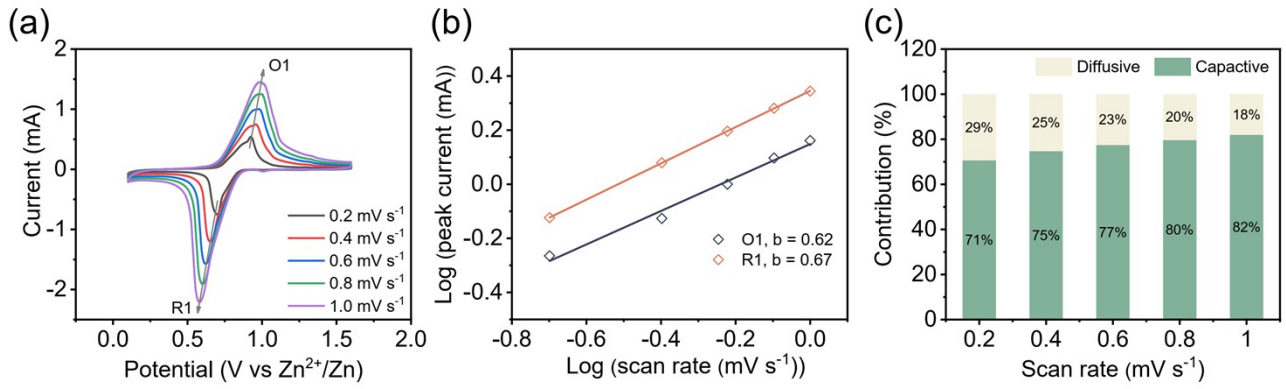

Figure S9. Kinetic study of MANQ electrode. (a) CV curves at different scan rates. (b) Log *i* versus log *v* plots to determine the *b* values of different peaks. (c) Capacitive contributions in CV curve at different scan rates.

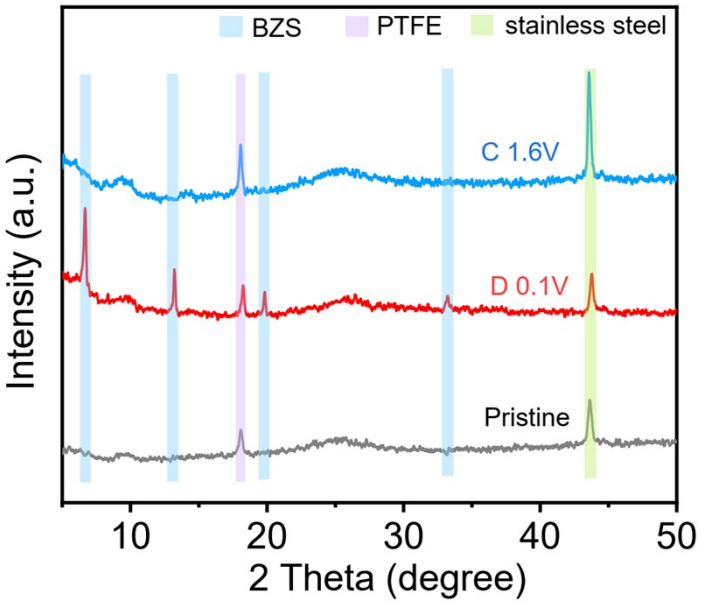

Figure S10. XRD patterns of TANQ electrodes at different states: pristine, discharged to 0.1 V and charged to 1.6 V. BZS: basic zinc salt, $Zn_x(OTF)_y(OH)_{2x-y}\cdot nH_2O$; PTFE: polytetrafluoroethylene binder.

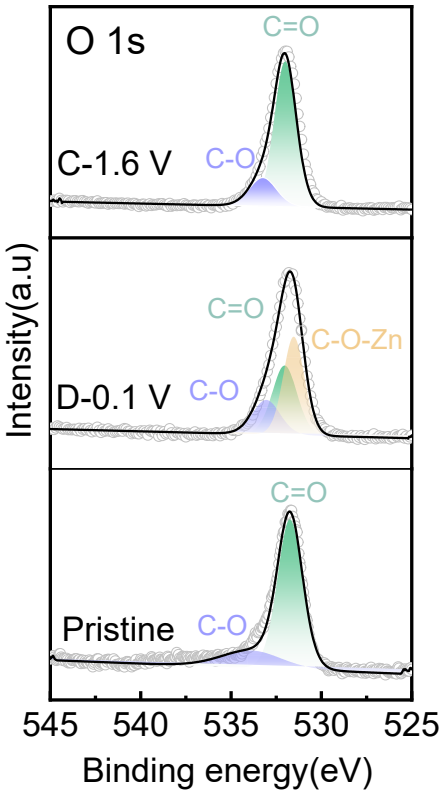

Figure S11. O 1s XPS spectra of the TANQ electrode during discharge and charge.

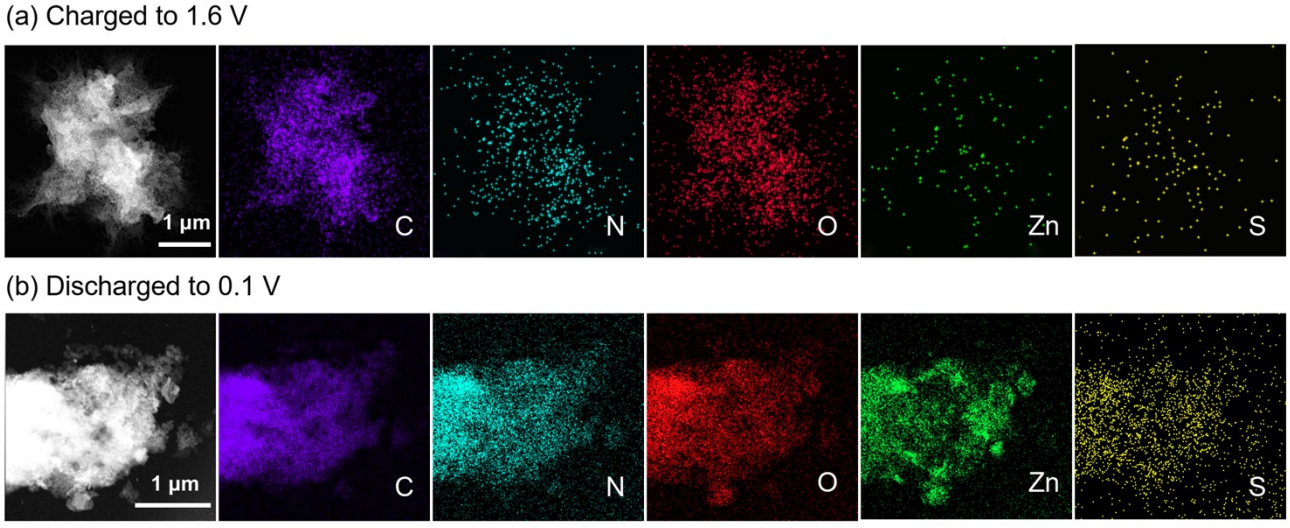

Figure S12. TEM-EDS mappings of C, N, O, Zn, and S element distributions on TANQ electrodes at different states: (a) charged to 1.6 V, (b) discharged to 0.1 V.

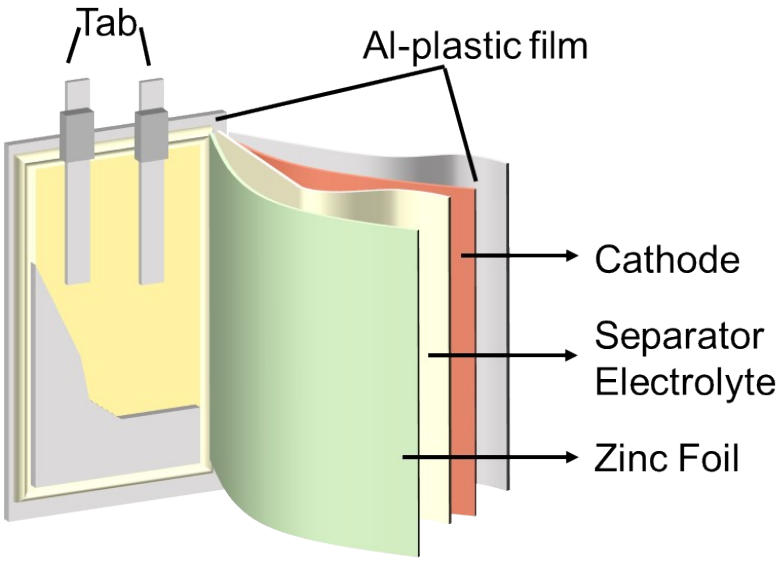

Figure S13. Schematic diagram of soft pack battery.

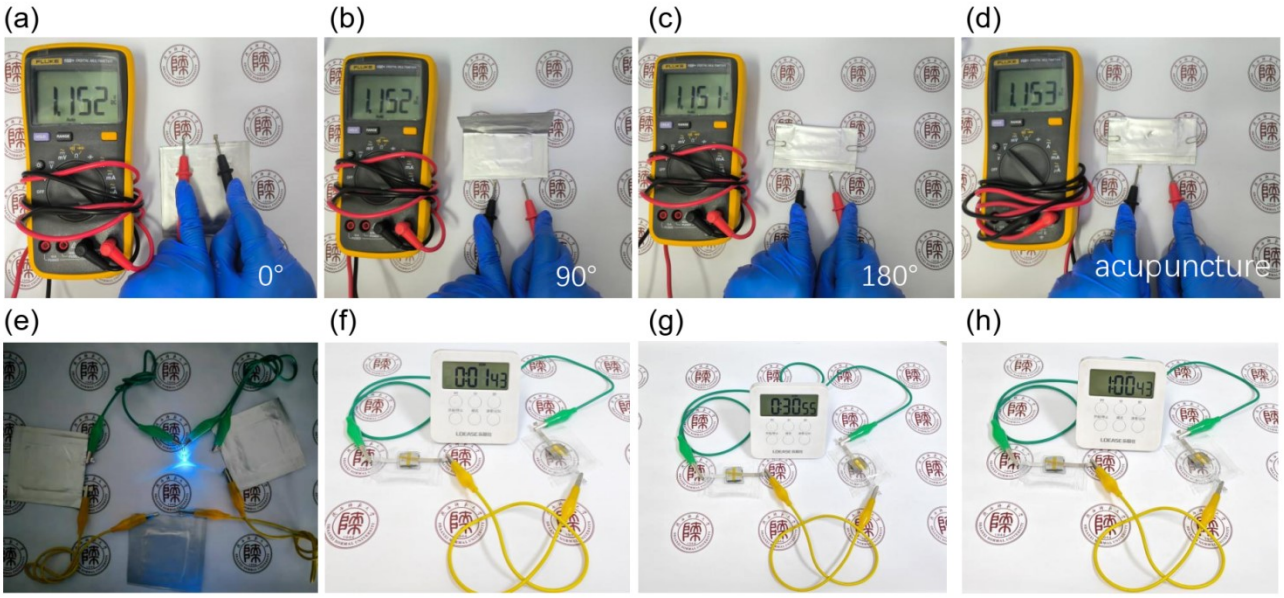

Figure S14. (a-d) Voltage stability of TANQ soft−pack battery under flat and different bending angles and acupuncture. (e) Three TANQ soft−pack batteries light up the LED. (f-h) Two TANQ soft−pack batteries assembled with gel electrolyte light up the timer.

Table S2. Electrochemical performance comparison of TANQ with previously reported organic cathodes for ZOBs.

Cathode Type	Cathodes	E (Wh kg^{-1})	Average Voltage (V vs. Zn/Zn^{2+})	Specific Capacity (mAh g^{-1})	Current Density (mA g^{-1})	Ref.
Organic Small Molecules	TANQ	141.05	0.65	217	200	This work
	AQ	92	0.49	188	20	S5
	PPPA	117.6	0.56	210.2	50	S6
	TRT	136	0.8	170	100	S7
	MB	83.2	0.8	104	167	S8
	DAPBQ	122.4	0.6	204	200	S9
	π-PMC	61.45	0.5	122.9	200	S10
	APh-NQ@CNT	131.3	0.65	202	100	S11
	BDB	140	1.25	112	390	S12
Organic Polymers	PDpBQH	138	1.15	120	100	S13
	Tannin-PANI	116.5	1	116.5	100	S14
	PTL	96	0.8	120	100	S15
	AOPs	136	0.8	170	500	S16
	PO	88.2	0.6	147	50	S17
	PNAQ/PNAQ	51	0.6	85	600	S18
	pEP(NQ)E/pEP(QH_2)E	24	0.4	60	225	S19
Porous framework structure	HKCO-DANT-COF	135.68	0.53	256	100	S20
	P_3Q-t	142.2	0.6	237	300	S21

Table S3. Comparison of diffusion coefficient between reported work and this work.

Cathode	Electrolyte	D (cm^2 s^{-1})	Ref.
BDPPDO	1 M $ZnSO_4$	10^{-9}~10^{-11}	S22
PDBS	2 M $ZnSO_4$	10^{-11}~10^{-10}	S23
PA-COF	1 M $ZnSO_4$	10^{-11}~10^{-8}	S24
$K_{0.41}MnO_2 \cdot 0.5H_2O$	2 M $ZnSO_4$ + 0.2 M $MnSO_4$	10^{-12}~10^{-9}	S25
GDAQ	2 M $ZnSO_4$	10^{-8}~10^{-12}	S26
TANQ	2 M $Zn(CF_3SO_3)_2$	10^{-9}~10^{-12}	This work

References

[S1] Frisch, M. J.; Trucks, G. W.; Schlegel, H. B.; Scuseria, G. E.; Robb, M. A.; Cheeseman, J. R.; Scalmani, G.; Barone, V.; Petersson, G. A.; Nakatsuji, H.; Li, X.; Caricato, M.; Marenich, A. V.; Bloino, J.; Janesko, B. G.; Gomperts, R.; Mennucci, B.; Hratchian, H. P.; Ortiz, J. V.; Izmaylov, A. F.; Sonnenberg, J. L.; Williams-Young, D.; Ding, F.; Lipparini, F.; Egidi, F.; Goings, J.; Peng, B.; Petrone, A.; Henderson, T.; Ranasinghe, D.; Zakrzewski, V. G.; Gao, J.; Rega, N.; Zheng, G.; Liang, W.; Hada, M.; Ehara, M.; Toyota, K.; Fukuda, R.; Hasegawa, J.; Ishida, M.; Nakajima, T.; Honda, Y.; Kitao, O.; Nakai, H.; Vreven, T.; Throssell, K.; Montgomery, J. A., Jr.; Peralta, J. E.; Ogliaro, F.; Bearpark, M. J.; Heyd, J. J.; Brothers, E. N.; Kudin, K. N.; Staroverov, V. N.; Keith, T. A.; Kobayashi, R.; Normand, J.; Raghavachari, K.; Rendell, A. P.; Burant, J. C.; Iyengar, S. S.; Tomasi, J.; Cossi, M.; Millam, J. M.; Klene, M.; Adamo, C.; Cammi, R.; Ochterski, J. W.; Martin, R. L.; Morokuma, K.; Farkas, O.; Foresman, J. B.; Fox, D. J., Gaussian, Inc., Wallingford, CT, USA, **2016**.

[S2] Lindström, H.; Södergren, S.; Solbrand, A.; Rensmo, H.; Hjelm, J.; Hagfeldt, A.; Lindquist, S.-E. Li^+ Ion Insertion in TiO_2 (Anatase). 2. Voltammetry on Nanoporous Films. *J. Phys. Chem. B* **1997**, *101*, 7717-7722.

[S3] Liu, T. C.; Pell, W. G.; Conway, B. E.; Roberson, S. L. Behavior of Molybdenum Nitrides as Materials for Electrochemical Capacitors: Comparison with Ruthenium Oxide. *J. Electrochem. Soc.* **1998**, *145*, 1882.

[S4] Li, H.; Chen, L.; Xing, F.; Miao, H.; Zeng, J.; Zhang, S.; He, X. Cross-linking enhances the performance of four-electron carbonylpyridinium based polymers for lithium organic batteries. *Chem. Sci.* **2024**, *15*, 14399.

[S5] Wang, Q.; Xu, X.; Yang, G.; Liu, Y.; Yao, X., An organic cathode with tailored working

potential for aqueous Zn-ion batteries. *Chem. Commun.* **2020**, *56*, 11859.

[S6] Ye, F.; Liu, Q.; Dong, H.; Guan, K.; Chen, Z.; Ju, N.; Hu, L., Organic Zinc-Ion Battery: Planar, π-Conjugated Quinone-Based Polymer Endows Ultrafast Ion Diffusion Kinetics. *Angew. Chem. Int. Ed.* **2022**, *61*, e202214244.

[S7] Wang, W.; Tang, Y.; Liu, J.; Li, H.; Wang, R.; Zhang, L.; Liang, F.; Bai, W.; Zhang, L.; Zhang, C., Boosting the zinc storage of a small-molecule organic cathode by a desalinization strategy. *Chem. Sci.* **2023**, *14*, 9033.

[S8] Tang, M.; Zhu, Q.; Hu, P.; Jiang, L.; Liu, R.; Wang, J.; Cheng, L.; Zhang, X.; Chen, W.; Wang, H., Ultrafast Rechargeable Aqueous Zinc-Ion Batteries Based on Stable Radical Chemistry. *Adv. Funct. Mater.* **2021**, *31*, 2102011.

[S9] Liu, X.; Tang, J.; Bin, D.; Wang, Y.; Li, C.; Su, L.; Shen, Y.; Hu, W.; Hu, Z.; Zhuang, W.; Yang, B.; Lu, H.; Wang, Y., Quinone-pyrazine organic cathode with intramolecular hydrogen bonds enabling high-charging and wide-temperature aqueous zinc batteries. *Energy Stor. Mater.* **2025**, *81*, 104517.

[S10] Zhang, H.; Fang, Y.; Yang, F.; Liu, X.; Lu, X., Aromatic organic molecular crystal with enhanced π–π stacking interaction for ultrafast Zn-ion storage. *Energy Environ. Sci.* **2020**, *13*, 2515.

[S11] Kumankuma-Sarpong, J.; Tang, S.; Guo, W.; Fu, Y., Naphthoquinone-Based Composite Cathodes for Aqueous Rechargeable Zinc-Ion Batteries. *ACS Appl. Mater. Interfaces* **2021**, *13*, 4084.

[S12] Glatz, H.; Lizundia, E.; Pacifico, F.; Kundu, D., An Organic Cathode Based Dual-Ion Aqueous Zinc Battery Enabled by a Cellulose Membrane. *ACS Appl. Energy Mater.* **2019**, *2*, 1288

[S13] Wang, X.; Xiao, J.; Tang, W., Hydroquinone versus Pyrocatechol Pendants Twisted Conjugated Polymer Cathodes for High-Performance and Robust Aqueous Zinc-Ion Batteries. *Adv.*

Funct. Mater. **2022**, *32*, 2108225.

[S14] Dong, H.; Wang, L.; Zhang, F.; Li, H.; Zhao, X.; Wei, W.; Kang, Y.; Yan, C.; Sang, Y.; Liu, H.; Wang, S., Green proton reservoirs of PANI for disposable high-performance zinc-ion batteries. *Nano Energy* **2024**, *128*, 109768.

[S15] Zhao, L.; Jia, Y.; Wu, Y.; Gu, T.; Zhou, X.; Wang, X.; Zhong, L.; Zhan, S.; Lv, H.; Zhi, C.; Liu, J., An Ultra-Stable 2D Linear Polymer Cathode for High-Performance Aqueous Zinc-Organic Batteries. *Angew. Chem. Int. Ed.* **2025**, *64*, e202425082.

[S16] Wang, Y.; Cui, H.; Li, R.; Yue, C.; Pan, H.; Tang, Z.; Wang, X.; Lin, Y.; Li, H.; Han, C.; Nan, D.; Zhi, C.; Lv, H., Bistate-type ion storage of azo polymer for aqueous zinc ion battery. *Energy Stor. Mater.* **2024**, *65*, 103102.

[S17] Tie, Z.; Deng, S.; Cao, H.; Yao, M.; Niu, Z.; Chen, J., A Symmetric All-Organic Proton Battery in Mild Electrolyte. *Angew. Chem. Int. Ed.* **2022**, *61*, e202115180.

[S18] Sun, T.; Du, H.; Zheng, S.; Shi, J.; Yuan, X.; Li, L.; Tao, Z., Bipolar Organic Polymer for High Performance Symmetric Aqueous Proton Battery. *Small Methods* **2021**, *5*, 2100367.

[S19] Strietzel, C.; Sterby, M.; Huang, H.; Strømme, M.; Emanuelsson, R.; Sjödin, M., An Aqueous Conducting Redox-Polymer-Based Proton Battery that Can Withstand Rapid Constant-Voltage Charging and Sub-Zero Temperatures. *Angew. Chem. Int. Ed.* **2020**, *59*, 9631.

[S20] Zhang, R.; Luo, D.; Xu, H.; Wang, J.; Dou, H.; Zhang, X., A polyarylimide covalent organic frameworks anode with ultralong discharge platform boosts high energy density Rocking-Chair Zn ion batteries. *Chem. Eng. J.* **2023**, *476*, 146741.

[S21] Wang, X.; Tang, J.; Tang, W., Manipulating Polymer Configuration to Accelerate Cation Intercalation Kinetics for High-Performance Aqueous Zinc-Ion Batteries. *Adv. Funct. Mater.* **2022**,

32, 2200517.

[S22] Shi, Y.; Chen, M.; He, W.; Xu, Z.; Gao, H.; Xu, J.; Cao, J., Enhanced electrolyte-wettability of organic cathode by introducing pyridine nitrogen atoms for high-performance aqueous zinc-ion batteries. *J. Power Sources* **2025,** *629*, 236022.

[S23] Sun, T.; Li, Z.-J.; Zhi, Y.-F.; Huang, Y.-J.; Fan, H. J.; Zhang, Q., Poly(2,5-Dihydroxy-1,4-Benzoquinonyl Sulfide) As an Efficient Cathode for High-Performance Aqueous Zinc–Organic Batteries. *Adv. Funct. Mater.* **2021**, *31*, 2010049.

[S24] Wang, W.; Kale, V. S.; Cao, Z.; Kandambeth, S.; Zhang, W.; Ming, J.; Parvatkar, P. T.; Abou-Hamad, E.; Shekhah, O.; Cavallo, L.; Eddaoudi, M.; Alshareef, H. N., Phenanthroline Covalent Organic Framework Electrodes for High-Performance Zinc-Ion Supercapattery. *ACS Energy Lett.* **2020**, *5*, 2256.

[S25] Sun, T.; Nian, Q.; Zheng, S.; Yuan, X.; Tao, Z., Water cointercalation for high-energy-density aqueous zinc-ion battery based potassium manganite cathode. *J. Power Sources* **2020**, *478*, 228758.

[S26] Yi, P.; Li, Z.; Ma, L.; Feng, B.; Liu, Z.; Liu, Y.; Lu, W.; Cao, S.; Fang, H.; Ye, M.; Shen, J., Eco-Friendly High-Performance Symmetric All-COF/Graphene Aqueous Zinc-Ion Batteries. *Adv. Mater.* **2024,** *36*, 2414379.